A high resolution TOF-PET concept with axial geometry and digital SiPM readout

Journal Article

Author(s):
Casella, Chiara; Heller, Matthieu; Joram, Christian; Schneider, Thomas

Contents lists available at ScienceDirect

Nuclear Instruments and Methods in Physics Research A
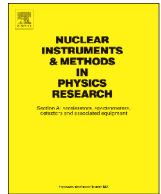
A high resolution TOF-PET concept with axial geometry and digital SiPM readout

C. Casella [a], M. Heller [b,*], C. Joram [b], T. Schneider [b]

[a] Institute for Particle Physics, ETH Zurich, CH-8093 Zurich, Switzerland
[b] CERN, PH Department, CH-1211 Geneva, Switzerland

ABSTRACT

The axial arrangement of long scintillation crystals is a promising concept in PET instrumentation to address the need for optimized resolution and sensitivity. Individual crystal readout and arrays of wavelength shifter strips placed orthogonally to the crystals lead to a 3D-detection of the annihilations photons. A fully operational demonstrator scanner, developed by the AX-PET collaboration, proved the potential of this concept in terms of energy and spatial resolution as well as sensitivity. This paper describes a feasibility study, performed on axial prototype detector modules with 100 mm long LYSO crystals, read out by the novel digital Silicon Photomultipliers (dSiPM) from Philips. With their highly integrated readout electronics and excellent intrinsic time resolution, dSiPMs allow for compact, axial detector modules which may extend the potential of the axial PET concept by time of flight capabilities (TOF-PET). A coincidence time resolution of 211 ps (FWHM) was achieved in the coincidence of two axial modules read out by dSiPMs, fully maintaining the demonstrated performance of the AX-PET detector.

1. Introduction

Positron Emission Tomography (PET) relies on the coincident detection of the two 511 keV photons originating from electron–positron annihilation. Inorganic scintillator crystals read out by photodetectors are used in the majority of PET detectors. The precise measurement of the time difference between the arrival times of the two photons allows to improve the PET performance: the annihilation point along the line of response (LoR) can be constrained and the time coincidence window reduced, leading to noise reduction and improved contrast in the reconstructed images. This concept, known as Time Of Flight (TOF)-PET, is usually implemented with short crystals, typically shorter than a few cm, read out by photomultipliers or SiPMs. Coincidence time resolutions in the range 400–600 ps FWHM have been achieved so far in commercial PET scanners [1], corresponding to a spatial constraint along the LoR of about 6–9 cm. Higher timing resolution has been obtained with prototype detectors, relying on various geometrical arrangement of fast scintillators, either with PMT [2,3] or SiPM readout [4–8]. Alternative detector concepts for TOF-PET systems based on the prompt emission of Cherenkov light are also being investigated [9,10].

The Digital Silicon Photomultiplier (dSiPM) technology [11–14] developed by Philips is receiving a growing interest for a wide range of photon counting applications, from high energy physics to medical imaging. Their excellent intrinsic time resolution and their high level of integration, which leads to unprecedented compactness, make these devices very attractive for PET detector systems, and particularly for TOF-PET. The absence of afterpulses and the potentially reduced dark count rate are an additional plus. Recent studies on the coincidence timing resolution achieved with short crystals coupled to dSiPM show resolutions around 120 ps FWHM [15].

Over the past few years, the AX-PET collaboration has developed a fully operational PET demonstrator [16], based on an axial geometrical approach: while in conventional PET systems, short scintillators point radially to the center of the tomograph, AX-PET uses long scintillator crystals (LYSO, 100 mm long, 3×3 mm^2 wide) which are arranged axially and stacked in several layers [17]. Arrays of wavelength shifter (WLS) strips are placed behind each layer of crystals. Hits in adjacent WLS strips define a cluster and its center of gravity provides the axial coordinate. Both the crystals and the WLS strips are individually read out by conventional SiPMs. Such a detector matrix allows for a 3D localization of the interactions of the 511 keV photons – both photoelectric absorption and Compton scattering – with good spatial resolution and sensitivity [18]. Two AX-PET detector modules have been constructed. They achieved competitive performance in terms of energy ($\Delta E/E \sim 12\%$, FWHM, at 511 keV) and spatial resolution

* Corresponding author. Tel.: +41 22 76 77786.
  E-mail address: matthieu.heller@cern.ch (M. Heller).

(< 2 mm, FWHM, in all 3 coordinates) [19]. Coincidence operation, followed by tomographic data analysis, resulted in parallax-error free reconstructed images of various phantoms and small animals (mice and rats) [20,21].

The work presented here focuses on experimental studies on 100 mm long axial crystals coupled to dSiPM photodetectors, as a proof of concept of an axial TOF-PET detector. The goal of the study is twofold. Firstly, it aims to demonstrate the feasibility of combining the new dSiPMs with an AX-PET like detector design. For this purpose, two small scale prototypes were built and characterized, based on the same detector concept as the AX-PET demonstrator, with crystals and WLS strips read out by dSiPMs. A critical aspect is the obtainable axial resolution which depends on the capability to read simultaneously relatively low light levels from several adjacent WLS strips. As a second step, the study explores the achievable time resolution of an axial set-up with long crystals read out on both sides by dSiPMs. The substantial propagation time of the scintillation photons inside the long crystals poses a particular challenge and the ultimate time resolution is obtained by a mean-timing method, which requires dual sided readout.

The paper is organized as follows: Section 2 describes the experimental set-ups and methods. It includes a summary of the main characteristics of the used dSiPM photodetectors and their most relevant operational aspects. Section 3 focuses on the achieved light yield and energy resolution from a simple test set-up, based on a single crystal. Section 4 is devoted to the full characterization of the two small scale modules based on the AX-PET detector concepts ("digital axial modules"), tested both individually and in coincidence. Timing measurements with two dual sided readout digital axial modules are detailed in Section 5. Finally, Section 6 reports coincidence timing measurements with small crystals ($3 \times 3 \times 3$ mm³), for comparison.

2. Experimental set-ups and methods

The digital axial PET detector modules were based on the same LYSO scintillator crystals and WLS strips as used in the AX-PET demonstrator. The dimensions of the crystals were ($3 \times 3 \times 100$) mm³ and of the WLS strips ($3 \times 0.9 \times 40$) mm³. For simplicity and cost reasons, the number of LYSO crystals per module was reduced to four, mounted in a 2×2 arrangement.

The crystals were either read out by a dSiPM at one end only (Fig. 1(a)), or on both ends (Fig. 1(b)). In the first case, a reflective Aluminium coating was deposited on the face opposite to the photodetector, to maximize the light yield. Sixteen WLS strips, arranged in a 2×8 geometry, were placed orthogonally behind the crystals with an air gap of 0.1 mm, covering only the central region along the axial direction. The LYSO crystals were not coated nor wrapped in order to allow a fraction of the scintillation light to escape from the crystal and to be absorbed by the WLS strips interleaved with the crystals. The optical coupling of crystals and WLS strips to the dSiPMs was provided by optical grease (Bicron BC-630). Behind each WLS strips layer, a white diffusive screen ensured light yield maximisation in the WLS strips and optical separation from the next crystal layer. For the timing measurements with dual sided readout (Fig. 1(b)) the axial coordinate was irrelevant and therefore the WLS strips were not readout, however left in place. For a fair comparison with the single sided readout set-up, the crystals were still not coated nor wrapped.

The modules were characterized with 511 keV annihilation photons from two different types of ^{22}Na sources: a "point-like" low activity source ($A = 178$ kBq, $\varnothing$ 250 μm), and a larger one, with higher activity ($A = 3.6$ MBq, $\varnothing$ 5 mm). The first one was used for all spatial resolution studies, where the smallest beam spot is required; the stronger source was used for the timing

studies, where the spatial resolution is not crucial and a higher count rate is preferred to reduce the duration of the data acquisition.

Prior to the coincidence measurements, the modules were individually characterized, in coincidence with a small scintillator crystal (LYSO, $3 \times 3 \times 3$ mm³, painted with white diffusive paint) read out by another dSiPM, used to tag the 511 keV photons. The required coincidence between the module and the tagger allows to confine the photon beam to a limited solid angle (defined by the size of the tagging crystal and the relative distances between tagger, source and module). Tagger and ^{22}Na source were aligned on a two-axis translation station in front of the module, such that the collimated beam spot could scan different positions across the crystals [19].

Temperature has a crucial impact on the operation of the dSiPMs, particularly in terms of dark count rate, as in most solid state devices. The dSiPMs were mounted and thermally coupled to an Aluminium frame, through which water at 15 °C was circulated in a buried channel.[1] During operation, the measured temperature on the dSiPMs was around 16.5 °C. The dSiPM used for the tagging crystal could not be cooled due to mechanical constraints.

2.1. The dSiPM detectors

Digital SiPM photodetectors of type DPC 3200-22-44 [14] were used for reading the light from the crystals and WLS strips. A dSiPM of type DPC 6400-22-44 [14] was used for the readout of the tagging crystal. Both types of detectors are arrays (also called *tiles*) of 8×8 digital photodetectors (called *pixels*), each of dimension 3.2×3.9 mm². Depending on the type of dSiPM detector, each pixel consists either of 3200 or 6400 digital cells, operated in Geiger avalanche mode. The 64 pixels are arranged on 16 identical units (called *dies*) of 4 pixels each. Each die operates independently from the others, although they are all connected to the same FPGA on the backside of the tile and share common services like e.g. the clock distributions. The discharged cells are summed up on a pixel basis; the die is the smallest readout unit of the dSiPM array, providing the counts of detected photons in its four pixels. Each die contains a pair of TDCs (19.5 ps time resolution) for the time measurement of the first detected photon(s). The close proximity of the TDCs to the diodes results in excellent intrinsic timing resolution. The data acquisition of a die is started by a *trigger*, generated when the number of detected photons per pixel exceeds a predefined threshold. For triggering purposes, the pixel is subdivided into four sub-pixels. The threshold can be set from one up to four detected photons. It is a *statistical* threshold, in the sense that it depends on the distribution of the photons in the sub-pixels (e.g. for trigger threshold equal to four, all four sub-pixels need to have at least one hit). For trigger thresholds other than one, the required effective number of fired cells is generally larger than the threshold value. Any of the four pixels can trigger the die. A single timestamp per die is produced when the trigger is satisfied. The readout of the die is started only if a second level trigger, the *validation*, is passed. As for the trigger, also the validation is a statistical threshold, which combines a threshold on the number of detected photons with their geometrical distribution inside the pixel. The main purpose of the validation step is to distinguish between scintillation events where the photon count will rapidly increase, and thermally generated dark noise events. If the validation is not passed within a predefined validation time window (from 5 to 40 ns), all cells of the die are recharged and – once the operation is completed – the die is ready to receive a new trigger. If the event is validated, an *integration* period is started, where the
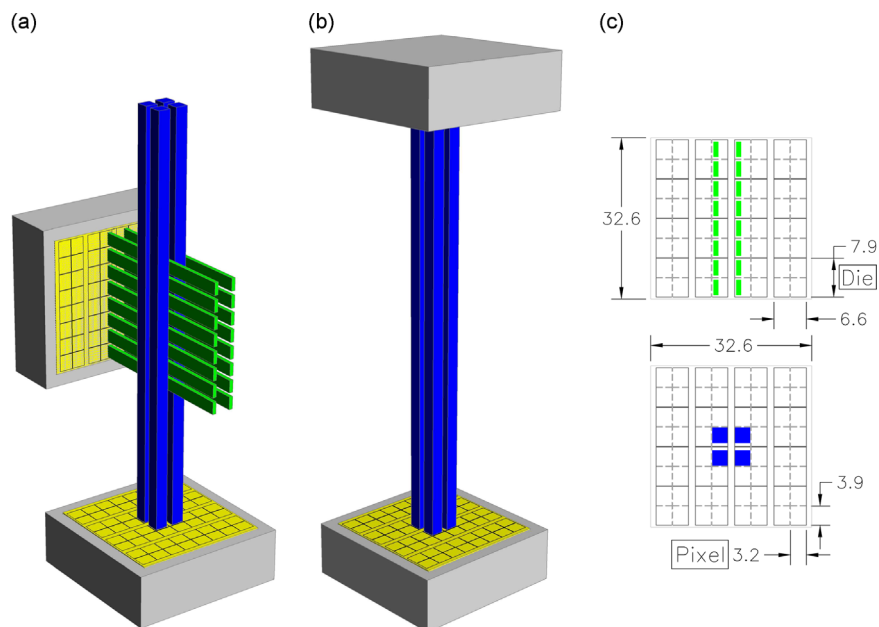
Fig. 1. Sketches of the "digital axial modules", with 4 LYSO crystals coupled to dSiPM photodetectors. (a) Single sided module used for the direct comparison with the AX-PET demonstrator, consisting of 2 layers of 2 crystals and 8 WLS strips each. (b) Dual sided axial module. (c) Geometrical positioning of the crystals and strips in the dSiPM tile. Only the cells covered by the detectors are activated in the dSiPM tile.

sensor waits and accumulates the incoming photons; at the end of the integration, the readout process sums the discharged cells. After readout, the cells are recharged and the die is ready for the next acquisition. The entire acquisition cycle duration is largely dominated by the readout time of 680 ns. Details of the dSiPM operation principle are provided in dedicated publications from Philips [11–14].

The data acquisition chain of the dSiPM detector is controlled by a *state machine*, implemented in the die and configurable by the FPGA. Its parameters (trigger and validation thresholds, duration of the various stages) are largely programmable. The achievable performance of a set-up read by dSiPMs depends crucially on the optimization of these settings for the respective measurement. To develop a thorough understanding of the various parameters and their interplay, a series of systematic tests was performed, in which the dSiPM tiles were exposed to light pulses from a LED. A detailed report on these measurements is available as a CERN technical note [22].

To achieve the ultimate timing precision in a scintillation detector, triggering on the first arriving photon is a commonly applied strategy. However, at ambient temperature, a low trigger threshold of 1 or 2 photons generates a rate of *dark triggers* in the kHz/cell (MHz/pixel) range. Even if these triggers are not validated, they cause a recharging of the die entailing a dead time (duration of the recharge process, programmable from 20 to 80 ns) that significantly reduces the die availability. This effect has a particular negative impact if one needs to read simultaneously several dies, as is the case for the WLS strips readout for the axial coordinate definition. In order to optimize the sensors availability, the dark count rate (DCR) must be minimized. The thermal generation of dark hits is most effectively suppressed by lowering the temperature. As in analog SiPMs, a temperature reduction by about 8 °C reduces the DCR by a factor of 2. Another action to reduce the DCR is to disable all unused cells that lie outside the footprint of a crystal or a WLS strip (see Fig. 1(c)). Those cells would contribute to the DCR, without having a chance to detect scintillation photons. Disabling them reduces the average DCR and increases the global availability of the die, without any unwanted side effect. In addition, the DCR of every cell can be determined individually and the highest dark count cells can be disabled. As an example,

a reduction in the average DCR by 50% is observed when disabling the 10% noisiest cells in the pixel, obviously also entailing a 10% reduction in photon detection efficiency. Studies of the performance of the dSiPM detectors at different percentages of disabled cells were done [22]. The measurements reported in the present paper were performed without any additional masking of the highest dark count cells, maintaining the photon detection efficiency at its maximum.

The dSiPM acquisition is done in frames of 327 μs [14]. Within each frame, the dies timestamps of all the tiles are synchronous allowing the offline building of the coincidences.

3. Light yield spectra and energy resolution

Prior to the measurements with the modules, a simple test setup with one LYSO crystal was used to define the typical light yield and energy resolution, both in the configuration of one single sided readout crystal (with Al coating) and with one crystal read out on both sides by dSiPMs. Fig. 2 shows the raw light yield spectra of a ^{22}Na source placed close to the crystals, in terms of number of detected photoelectrons i.e. fired cells. In the dual sided readout case (Fig. 2, bottom) the light yield summed over the two tiles and the one recorded by one tile only are both shown. The direct comparison of the one tile spectra demonstrates in first approximation the effect of the Al coating in increasing the light yield.

In order to get an estimate of the real number of photons detected by the dSiPM, the recorded light yield should be corrected both for the non-linearity of the photodetectors (due to the limited number of cells), and for the cross talk effects. The cross talk is induced by optical photons which are emitted from the Geiger avalanche in a cell. Those photons can provoke other avalanches in neighboring cells in the same pixel (inter-cells cross talk). At the same time, they can also propagate through the crystal, and either be detected by the photodetector, after reflection from the Al coating (for single sided readout crystals), or be detected by the opposite photodetector (in the dual sided readout configuration). Both types of cross talk – inter-cell and through-crystal cross talk – effectively increase the number of detected fired cells, enhancing the true
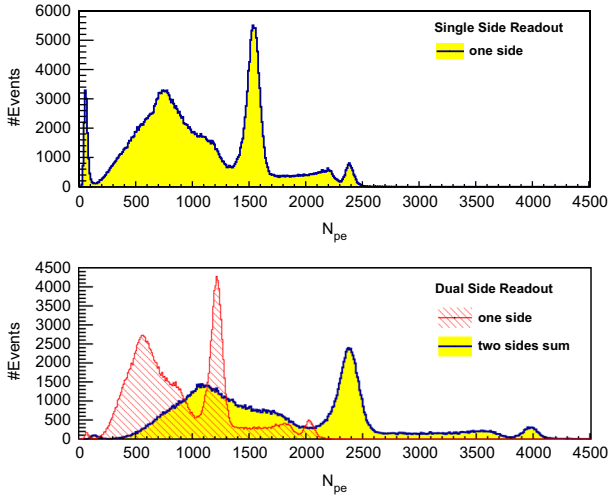
Fig. 2. Light yield spectra – in numbers of detected photoelectrons – of two different 100 mm long LYSO crystals exposed to photons from a ^{22}Na source, both in single sided readout crystal with Al coating (top) and in a dual sided readout crystal (bottom). In the dual sided readout, the two tiles were acquired in coincidence, resulting also in a significant reduction of the dark count contribution (peak at low N_{pe}).
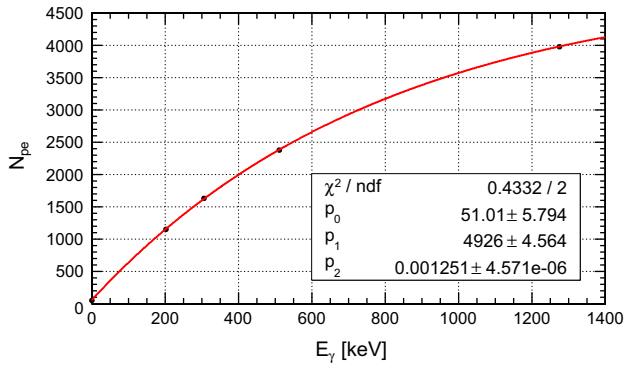

Fig. 3. Number of photoelectrons detected in the dSiPM as a function of the deposited energy, for the energy calibration of the dual sided readout crystal. The energy points correspond to the gamma emission of the ^{22}Na source (511 keV and 1275 keV) and LYSO intrinsic radioactivity (202 keV and 307 keV).

photoelectric yield. The correct determination of the photoelectric yield requires a model which accounts for all effects (non-linearity and both types of cross talk). Such a correction was not applied to the presented measurements, and the light yields are quoted as raw numbers of detected photoelectrons.

An energy calibration was performed, as shown in Fig. 3, plotting the number of detected photoelectrons N_{pe} as a function of the energy E_γ, modelled by a simple exponential function:

$$N_{pe} = p_0 + p_1 \left(1 - e^{-p_2 E}\right). \tag{1}$$

The two energy lines of the ^{22}Na source (511 keV and 1275 keV) and the intrinsic radioactivity of the LYSO (202 keV and 307 keV) were used. The energy calibration method is detailed in Ref. [19]. By construction, the energy calibration leads to an energy spectrum where non-linearity and cross talk effects are corrected for. After calibration, energy resolutions $\Delta E/E = (14.2 \pm 0.1)\%$ and $\Delta E/E = (12.6 \pm 0.1)\%$ FWHM, at 511 keV, are obtained respectively for the single sided and dual sided readout. The improved energy resolution for the dual sided readout is a direct consequence of the increased light yield.

4. Digital axial modules with WLS strips

As described in Section 2, two small scale AX-PET like digital modules were built, using 4 LYSO crystals and 16 WLS strips per module, arranged in two layers and coupled to dSiPMs (Fig. 1(a)). Their performance was assessed, firstly one module at the time with the electronically collimated photons beam, and then by putting the two modules in coincidence.

The 4 LYSO crystals were positioned on four different dies, logically decoupling their readout. The trigger level was set to 4 photons for spatial resolution measurements (Section 4.1) while it was set to 1 for timing measurements (Section 4.2). The validation was set to the highest possible value, i.e. 8. The measured light yield – averaged over the 8 crystals of the two modules – was 1326 photoelectrons at 511 keV energy deposition with an RMS of 118 pe. The significant RMS value is due to imperfections of the optical coupling with grease.

The 2×8 WLS strips were placed on 16 different pixels belonging to 8 different dies. As the WLS information is not relevant for the time resolution, the trigger threshold was set to 2. The validation pattern was optimized for the shape and size of the WLS footprint and corresponded to a statistical threshold of 6 photons. Special operating options (i.e. refresh option and neighboring logic) were used specifically for the WLS strips readout, in order to have a die availability close to 100% and recover the full cluster information. Details about all the settings used in the dSiPMs for the WLS strips readout are given in Ref. [22].

4.1. Axial resolution

Clusters of WLS strips were reconstructed, consisting on average of 3 strips, with a total light yield around 100 pe, comparable with the AX-PET demonstrator result [19]. The axial resolution on the individual modules was measured following the procedure described in Ref. [19], using a photon beam collimated with the tagging crystal. An axial resolution of 1.30 mm FWHM was obtained with the beam pointing in the centre of the WLS strip, while 1.85 mm FWHM was measured with the beam centered in between the two strips. The modulation is due to the pitch in the WLS strips (4 mm pitch, with a 1 mm wide gap between the strips, compared to the 3.2 mm pitch and 0.2 mm gap in AX-PET). A single module resolution of 1.57 mm FWHM is quoted as the average of the two numbers.

Once characterized individually, the two modules were mounted face-to-face, at a distance of 150 mm, and read out in coincidence, with the ^{22}Na source placed in between. The lines of response connecting the detections points were drawn and their intercept with the confocal plane calculated, as shown in Fig. 4. The projection of the intersection points along the axial direction measures the axial resolution of the two modules operated in coincidence [19]. Subtracting in quadrature the finite positron range, the non-collinearity term and the source size, an axial resolution of 1.21 mm FWHM is obtained. The result agrees with the single module resolution quoted above.

4.2. Coincidence time resolution

With the two modules used in coincidence, the coincidence resolving time (CRT) was measured as the FWHM of the time difference distribution. The fact that the Geiger discharge is a very fast process and constrained to the thin high field region, combined with the high resolution of the dSiPM TDC electronics and with the high photoelectric yields reported above, promises an excellent CRT. However, the axial dependent light propagation times in the long LYSO crystals spoil the result, unless it can be corrected for.
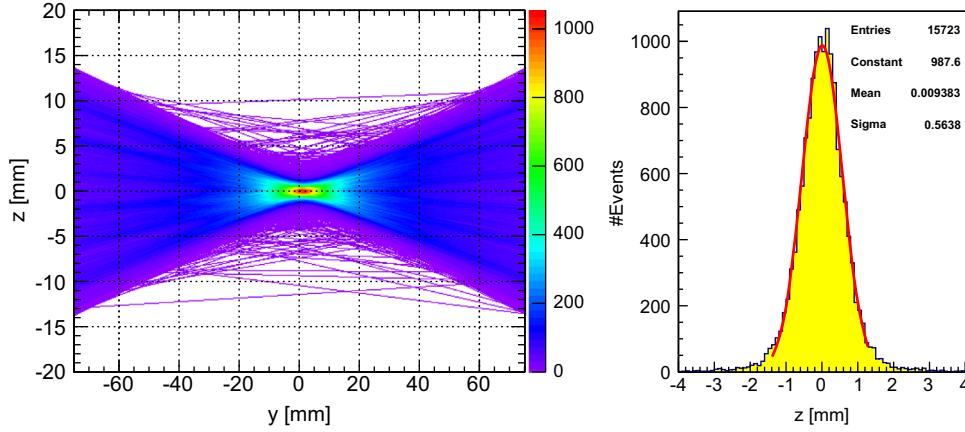
Fig. 4. Left: drawing of the lines of response from the coincidence of two digital axial modules i.e. confocal (non-tomographic) reconstruction of the ^{22}Na source. Right: projection along the axial (z) direction of the intersection of the lines of response with the central plane, as measurement of the axial spatial resolution.
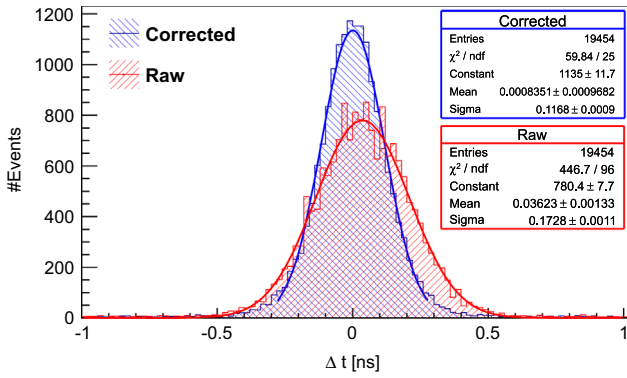

Fig. 5. Time difference distribution for all the 16 crystal pairs merged together, both before and after timing correction. Only photoelectric events are selected.

Fig. 6. Example of light path calibration for one crystal combination.

Fig. 5 shows the time difference between pairs of crystals of the two modules, for all 16 combinations (4 crystals per module, 2 modules, 4×4 possible pairs of coincidences). The same distribution is shown both uncorrected and after correction for the axial coordinate. Only the events with a photoelectric interaction in the axial range which is covered by WLS strips are used for the CRT measurement. A CRT of ~ 406 ps FWHM prior to correction improves to ~ 274 ps FWHM after correction, in perfect agreement with the value obtained from the average of the 16 crystal combinations, fitted independently: 274 ps FWHM with an RMS of 38 ps.

The time correction for the light path in the crystal was applied on an event-by-event basis, relying on the axial coordinate information from the WLS strips. For each of the 16 crystal combinations, the time difference between the two modules (Δt) was plotted versus the difference of the reconstructed axial coordinates (Δz), as shown in Fig. 6. The intercept p_0 of the linear fit is related to an internal time offset between the trigger networks of the respective dies. The slope p_1 represents the inverse of the effective light propagation speed s:

$$\frac{1}{p_1} = s = k \frac{c}{n} \tag{2}$$

where c is the speed of light in vacuum, n is the LYSO refractive index ($n = 1.8$) and k is a geometrical factor. The latter expresses the fact that most of the photons do not propagate on a straight line but by bouncing repeatedly from the crystal sides. As a consequence, a smaller speed is obtained when projected along the crystal length (*effective* speed). Averaged over the 16 crystal combinations, a slope of 7.5 ps/mm and an effective speed of about 0.13 mm/ps are obtained, corresponding to a geometrical factor k of 0.8.
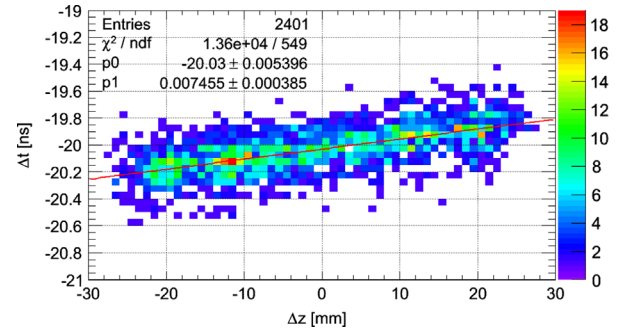
5. Digital axial modules with dual sided readout

The dual sided readout of the scintillation crystals (Fig. 1(b)) allows the calculation of a mean time per crystal, t_m:

$$t_m = \frac{t_{up} + t_{down}}{2} \tag{3}$$

which, by construction, is independent of the axial coordinate (*up* and *down* represent the two readout positions).

5.1. Dual sided module with tagger

The two dual sided readout modules were characterized, one at the time, in coincidence with the tagging crystal. A total light yield – from the sum of the two readout sides – of about 2159 photoelectrons with an RMS of 93 pe was measured, averaged over the 8 crystals of the two modules.

Fig. 7 shows the timing difference distribution for the four LYSO crystals of the module, merged together, when the tagger is placed in the central axial position. A CRT of ~ 208 ps FWHM was obtained from this merged distribution. The average of the contribution of the four crystals treated separately gives a CRT of (197 ± 13) ps FWHM.

The timing performance was studied as a function of the axial position of the beam spot, as summarized in Fig. 8, confirming that both the module mean time and the CRT are independent of the axial coordinate, as expected. From the axial scan, a slope of ~ 7.5 ps/mm was also extracted from the time difference between the single side readout and the tagger (e.g. $t_{up} - t_{tag}$) as a function of the axial coordinate. Equivalently, a slope of ~ 15 ps/mm is measured when the time difference between the two readout sides (i.e. $t_{up} - t_{down}$) is plotted versus the axial coordinate, with an
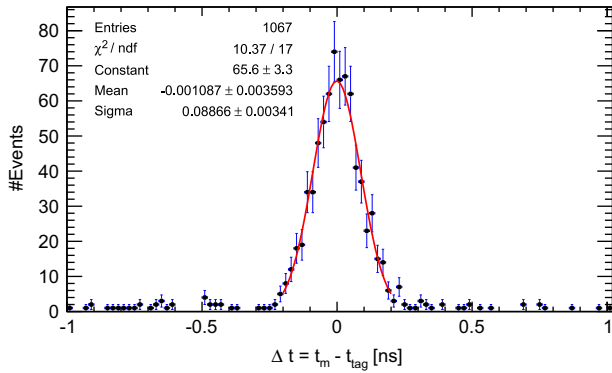
Fig. 7. Time difference distribution between the crystal mean time (t_m) and the time of the tagging crystal (t_{tag}). The plot merges together the results of the 4 LYSO crystals of the dual sided readout module. The tagger is placed in the central axial position. Only photoelectric events are selected.
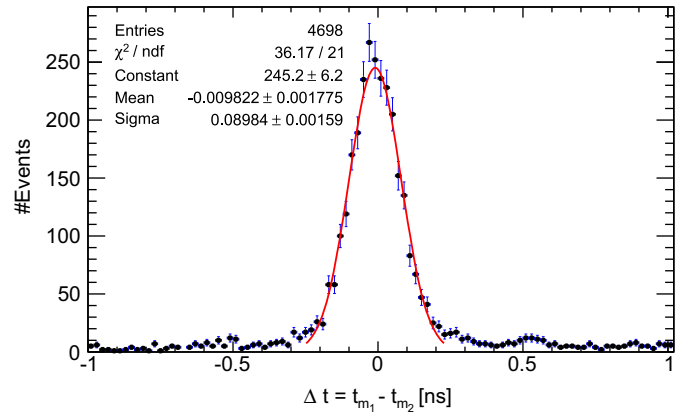

Fig. 9. CRT measurement for the two dual sided readout modules in coincidence using the mean time method. The plot refers to all 16 possible combinations of LYSO crystals pairs, merged together. Only photoelectric events are selected.
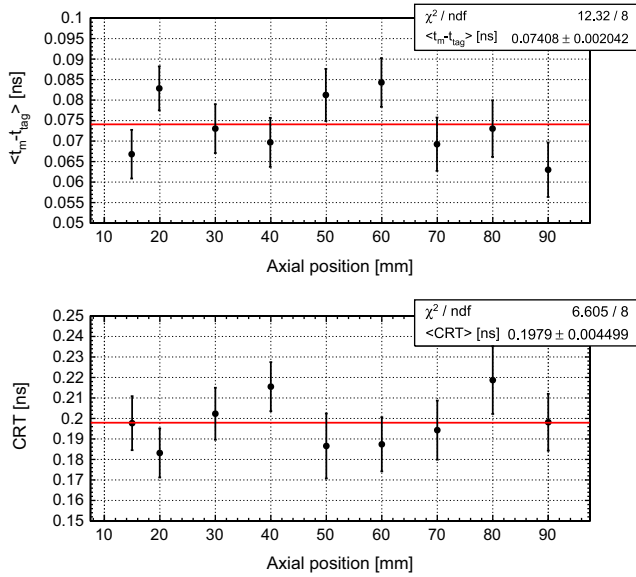

Fig. 8. Mean value of the module-tagger time difference distribution (top) and corresponding CRT FWHM (bottom) as a function of the axial position of the tagging crystal. The graphs refer to one LYSO crystal of the dual sided readout module.

Fig. 10. CRT for the two dual sided readout modules coincidence setup as a function of the position of the source in between the two modules. The distance between the modules is 30 cm. Position 0 corresponds to the source exactly in the middle of this distance.

average CRT of about 294 ps FWHM. This result is in perfect agreement with the already quoted effective propagation speed inside the 100 mm long LYSO crystals (Section 4.2).

5.2. Coincidence of two dual sided readout modules

Two dual sided readout modules were mounted face-to-face and read out in coincidence, with the ^{22}Na source positioned in between. The mean time of every crystal was calculated. The time difference was measured for every pair of crystals in the two modules. Fig. 9 shows the merged distribution from which a CRT of ~ 211 ps FWHM is measured. In a TOF-PET, such a CRT would correspond to a constraint along the LoR of $\Delta x = (c/2)\Delta t = 3.1$ cm FWHM. The CRT computed as the average value of all 16 possible combinations is (215 ± 26) ps FWHM.

The CRT was measured for several horizontal positions of the source in between the two modules, keeping the source always in the same central axial (i.e. vertical) position. Fig. 10 shows the results of the horizontal scan proving that the CRT is fully independent of the source position.

The timing information alone – combined with the measured CRT – is obviously not sufficient to reconstruct the absolute position of
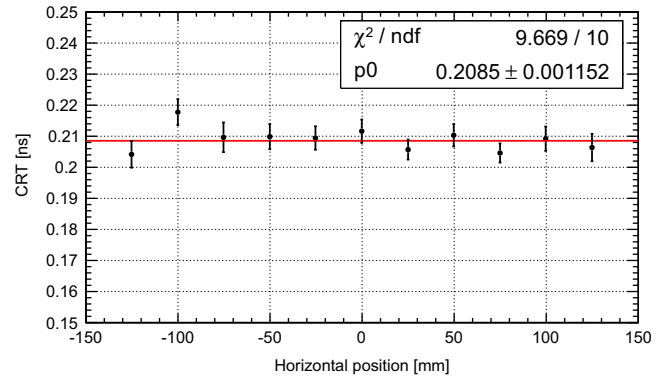
the interaction on an event by event basis. Nevertheless, in a lab test set-up with a point-like source, the position derived from the mean value of the time difference distribution is perfectly correlated with the real position of the source, as shown in Fig. 11. For all 16 combinations of LYSO crystal pairs in the two modules, the slope of the reconstructed vs nominal position equals 1.

6. Measurements with small size crystals

In order to further explore the timing performance of a LYSO-based detector with dSiPM readout, two small size LYSO crystals of $3 \times 3 \times 3$ mm^3 size, painted with white diffusive paint and coupled to separated DPC 3200-22-44 dSiPM tiles, were read out in coincidence. A ^{22}Na source was placed in between the two tiles. The trigger on the first photon was used, together with a validation threshold of 8. The tiles were cooled at 10 $^\circ$C with a Peltier unit and an average operation temperature of ~ 15.5 $^\circ$C was measured on the tiles. All the cells were activated to maximize the PDE. Typical uncorrected light yields of the order of ~ 2000 photoelectrons were observed from the crystals, at 511 keV energy deposition. A CRT of (133.2 ± 3.5) ps FWHM was measured from the time difference recorded by the two tiles in coincidence events, with an energy cut at the photopeaks (see Fig. 12). CRT deteriorated significantly if cooling was not used.

7. Conclusions

Two different types of axial PET modules based on long LYSO crystals with digital SiPM readout were built and characterized. The main results in terms of light yield and timing resolutions are summarized in Table 1.
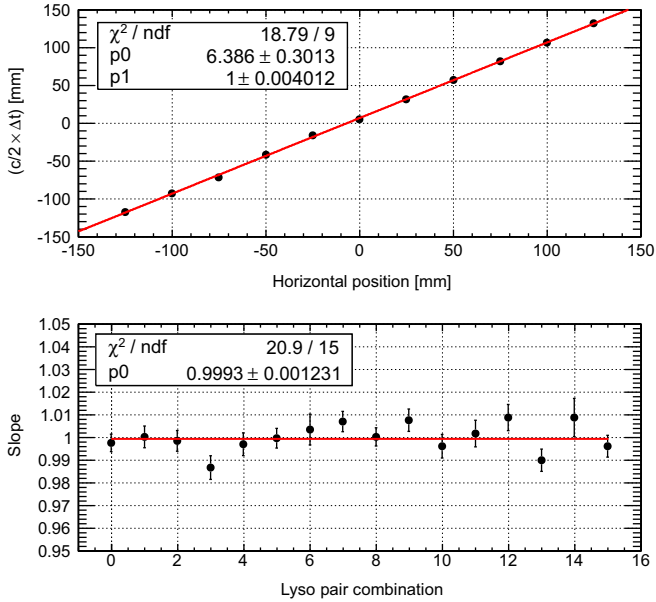

Fig. 11. Top: mean value of the reconstructed coordinate from TOF ($(c/2)\Delta t$) vs the nominal position, for one possible combination of crystals pairs. Bottom: resulting slopes of the TOF-reconstructed versus true coordinates, for all possible 16 crystals pairs.
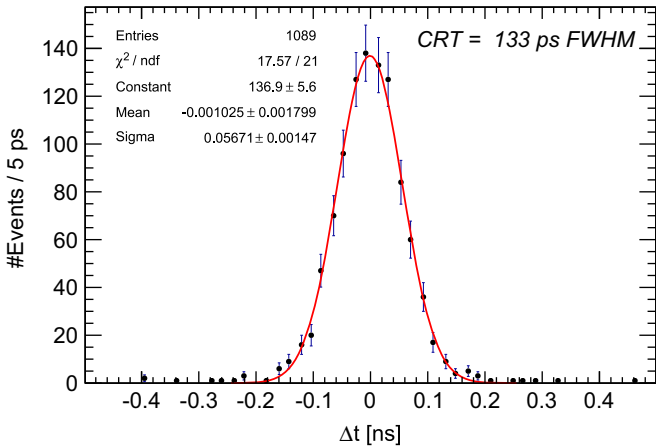

Fig. 12. CRT measurement using two $3 \times 3 \times 3$ mm^3 LYSO crystals. The DLS 3200 sensors are used with triggering on the first photon. Only photoelectric events are selected.

The measurements with two modules with single sided crystal readout and WLS strips demonstrated the general feasibility of the axial geometry, combined with the dSiPM readout, which requires the simultaneous readout of crystals and the associated clusters of WLS strips. The performance of the digital module was demonstrated to be fully comparable to the analog module of the AX-PET detector.

A moderate cooling and the optimization of the dSiPM operational parameters allowed to operate the reduced scale modules in an efficient way. However, for a full scale AX-PET system which requires simultaneous availability of several readout channels, the currently available dSiPM sensors and readout kit would not lead to an adequate system sensitivity, mainly due to dark counts induced dead time and the long readout sequence.

Excellent coincidence resolving times have been demonstrated with short scintillation crystals (CRT $\sim$ 130 ps FWHM), in which the fluctuations of the photon path length are of secondary importance. This is one of the most competitive timing measurements ever achieved with LYSO, or the equivalent LSO [6–8,15]. The dSiPM exceeds the timing performance of the best photomultipliers and is at least fully competitive with analog SiPMs equipped with ultrafast readout electronics. The digital concept with the TDCs integrated on the die level allows for excellent intrinsic timing resolution and guarantees easy scalability without performance loss.

When long crystals are considered, high resolution CRT demands an effective correction of the path length. A precise correction can be derived from the knowledge of the axial coordinate based on the WLS strip information. An even more powerful tool is the dual sided readout with the mean timing method, which, by construction, eliminates the axial dependence of the path length and leads to ultimate timing performance. A CRT of 211 ps (FWHM), constant over the full field of view, constrains the annihilation point on the LoR to 3.1 cm (FWHM), proving the principle of an axial TOF-PET with long crystals.

The result shows also that a novel positron emission imaging system, able to reconstruct the annihilation point along the LoR from TOF information alone (i.e. without the need of tomographic reconstruction), would still require a timing performance gain by one order of magnitude. Timing resolutions in the 10 ps range would also allow building an axial system with dual sided crystal readout in which the axial coordinate is reconstructed with competitive precision from the time difference of the two ends. This would make the WLS strip arrays obsolete for the axial coordinate definition and lead to a significant gain in simplicity, compactness and finally also cost effectiveness.

Acknowledgments

Table 1

Summary of the LYSO light yield and timing resolution of the two digital axial modules set-ups (single sided readout with WLS strips, and dual sided readout). The module intrinsic timing resolution is extracted from the measured coincidence resolving time from the two modules used in coincidence. Also the energy resolution is reported in the last column of the table, although extracted from a different setup of a single LYSO crystal not mounted in the module.

Module under test	Light yield [pe]		Measured CRT from coinc. setup [ps]	Module timing resolution [ps]	$\Delta E/E_{FWHM}$ (511 keV) (single crystal) (%)
	Mean	RMS			
Digital axial module with WLS strips	1326	118	274 (Fig. 5)	194 ($= 274/\sqrt{2}$)	14.2
Digital axial module with dual sided readout	2159	93	211 (Fig. 9)	149 ($= 211/\sqrt{2}$)	12.6

References

[1] M. Conti, Eur. J. Nucl. Med. Mol. Imaging 38 (6) (2011) 1147.
[2] W.W. Moses, et al., IEEE Trans. Nucl. Sci. NS-57 (3) (2010) 1570.
[3] J.P. Lee, et al., Biomed. Eng. Lett. 1 (2011) 174.
[4] S. Seifert, et al., Phys. Med. Biol. 57 (2012) 2219.
[5] C.L. Kim, et al., IEEE Trans. Nucl. Sci. NS-56 (2009) 2580.
[6] S. Seifert, et al., IEEE NSS MIC Conference Record (10.1109/NSSMIC.2009.5402260), 2009.
[7] J.Y. Yeom, et al., Phys. Med. Biol. 58 (2013) 1207.
[8] S. Gundacker, et al., in: Proceedings of Science, International Workshop on New Photon Detectors, LAL Orsay, France, 2012 〈http://pos.sissa.it/archive/conferences/158/016/PhotoDet%202012_016.pdf〉.
[9] R. Dolenec, Time-of-flight positron emission tomography using Cherenkov radiation (Ph.D. thesis), University of Ljubljana, 2013.
[10] T. Ooba, et al., IEEE NSS Conference Record, 2004.
[11] T. Frach, et al., IEEE NSS MIC Conference Record N28-005, 2009.
[12] T. Frach, et al., IEEE NSS MIC Conference Record N58-001, 2010.
[13] C. Degenhardt, et al., IEEE NSS MIC Conference Record (10.1109/NSSMIC.-2010.5874115), 2011.
[14] PDPC-TEK User Manual (v0.17), Philips Digital Photon Counting.
[15] H.T. van Dam, Phys. Med. Biol. 58 (2013) 3243.
[16] 〈http://cern.ch/ax-pet 〉.
[17] J. Seguinot, et al., Il Nuovo Cimento C 29 (2005) 429.
[18] A. Braem, et al., Nucl. Inst. Methods Phys. Res. A 586 (2008) 300.
[19] P. Beltrame, et al., Nucl. Inst. Methods Phys. Res. A 654 (2011) 546.
[20] E. Bolle, et al., IEEE NSS MIC Conference Record MIC22-5, 2011.
[21] C. Joram et al., Imaging results and TOF studies with axial PET detectors, Nuclear Instruments Methods in Physics Research A, ISSN. 0168–9002, http://dx.doi.org/10.1016/j.nima.2013.05.030.
[22] M. Heller, et al., CERN PH-EP-Tech-Note-2013-003, 2013.